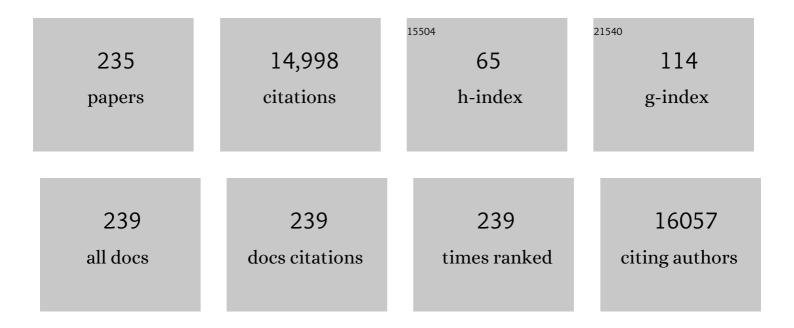
List of Publications by Year in descending order

Source: https://exaly.com/author-pdf/5648563/publications.pdf Version: 2024-02-01



SHUO CHEN

#	Article	IF	CITATIONS
1	Graphene oxide modified g-C ₃ N ₄ hybrid with enhanced photocatalytic capability under visible light irradiation. Journal of Materials Chemistry, 2012, 22, 2721-2726.	6.7	687
2	Facile Ammonia Synthesis from Electrocatalytic N ₂ Reduction under Ambient Conditions on N-Doped Porous Carbon. ACS Catalysis, 2018, 8, 1186-1191.	11.2	520
3	Efficient Electrochemical Reduction of Carbon Dioxide to Acetate on Nitrogen-Doped Nanodiamond. Journal of the American Chemical Society, 2015, 137, 11631-11636.	13.7	458
4	High‥ield Electrosynthesis of Hydrogen Peroxide from Oxygen Reduction by Hierarchically Porous Carbon. Angewandte Chemie - International Edition, 2015, 54, 6837-6841.	13.8	419
5	Graphene Sheets Grafted Ag@AgCl Hybrid with Enhanced Plasmonic Photocatalytic Activity under Visible Light. Environmental Science & Technology, 2011, 45, 5731-5736.	10.0	393
6	Enhanced activation of peroxymonosulfate by nitrogen doped porous carbon for effective removal of organic pollutants. Carbon, 2017, 115, 730-739.	10.3	372
7	Uncovering the Key Role of the Fermi Level of the Electron Mediator in a Z-Scheme Photocatalyst by Detecting the Charge Transfer Process of WO ₃ -metal-gC ₃ N ₄ (Metal = Cu, Ag, Au). ACS Applied Materials & Interfaces, 2016, 8, 2111-2119.	8.0	334
8	Vertically Aligned Janus MXene-Based Aerogels for Solar Desalination with High Efficiency and Salt Resistance. ACS Nano, 2019, 13, 13196-13207.	14.6	280
9	Enhanced Photocatalytic H ₂ O ₂ Production over Carbon Nitride by Doping and Defect Engineering. ACS Catalysis, 2020, 10, 14380-14389.	11.2	265
10	Selective electroreduction of CO2 to acetone by single copper atoms anchored on N-doped porous carbon. Nature Communications, 2020, 11, 2455.	12.8	265
11	Enhanced Fenton-like catalysis by iron-based metal organic frameworks for degradation of organic pollutants. Journal of Catalysis, 2017, 356, 125-132.	6.2	256
12	Enhanced H2O2 production by selective electrochemical reduction of O2 on fluorine-doped hierarchically porous carbon. Journal of Catalysis, 2018, 357, 118-126.	6.2	252
13	Heterogeneous activation of peroxymonosulfate by LaCo1-xCuxO3 perovskites for degradation of organic pollutants. Journal of Hazardous Materials, 2018, 353, 401-409.	12.4	249
14	CO ₂ Electroreduction at Low Overpotential on Oxide-Derived Cu/Carbons Fabricated from Metal Organic Framework. ACS Applied Materials & Interfaces, 2017, 9, 5302-5311.	8.0	239
15	Selective Electrochemical Reduction of Carbon Dioxide to Ethanol on a Boron―and Nitrogenâ€Coâ€doped Nanodiamond. Angewandte Chemie - International Edition, 2017, 56, 15607-15611.	13.8	226
16	TiO ₂ â^'Multiwalled Carbon Nanotube Heterojunction Arrays and Their Charge Separation Capability. Journal of Physical Chemistry C, 2007, 111, 12987-12991.	3.1	222
17	Photocatalytic Oxidation of Aqueous Ammonia Using Atomic Single Layer Graphitic-C ₃ N ₄ . Environmental Science & Technology, 2014, 48, 11984-11990.	10.0	204
18	Review of Fluorescence Suppression Techniques in Raman Spectroscopy. Applied Spectroscopy Reviews, 2015, 50, 387-406.	6.7	201

#	Article	IF	CITATIONS
19	Device Postannealing Enabling over 12% Efficient Solutionâ€Processed Cu ₂ ZnSnS ₄ Solar Cells with Cd ²⁺ Substitution. Advanced Materials, 2020, 32, e2000121.	21.0	201
20	Selective Electrochemical Reduction of Carbon Dioxide to Ethanol on a Boron―and Nitrogenâ€Coâ€doped Nanodiamond. Angewandte Chemie, 2017, 129, 15813-15817.	2.0	196
21	Enhancement of Catalytic Activity Over the Iron-Modified Ce/TiO ₂ Catalyst for Selective Catalytic Reduction of NO _{<i>x</i>} with Ammonia. Journal of Physical Chemistry C, 2012, 116, 25319-25327.	3.1	189
22	Efficient photo-Fenton activity in mesoporous MIL-100(Fe) decorated with ZnO nanosphere for pollutants degradation. Applied Catalysis B: Environmental, 2019, 245, 428-438.	20.2	187
23	Efficient Mineralization of Perfluorooctanoate by Electro-Fenton with H ₂ O ₂ Electro-generated on Hierarchically Porous Carbon. Environmental Science & Technology, 2015, 49, 13528-13533.	10.0	174
24	Improved Photocatalytic Performance of Heterojunction by Controlling the Contact Facet: High Electron Transfer Capacity between TiO ₂ and the {110} Facet of BiVO ₄ Caused by Suitable Energy Band Alignment. Advanced Functional Materials, 2015, 25, 3074-3080.	14.9	164
25	Atomic single layer graphitic-C ₃ N ₄ : fabrication and its high photocatalytic performance under visible light irradiation. RSC Advances, 2014, 4, 624-628.	3.6	152
26	Sputtered and selenized Sb2Se3 thin-film solar cells with open-circuit voltage exceeding 500ÂmV. Nano Energy, 2020, 73, 104806.	16.0	152
27	Adsorption of ciprofloxacin, bisphenol and 2-chlorophenol on electrospun carbon nanofibers: In comparison with powder activated carbon. Journal of Colloid and Interface Science, 2015, 447, 120-127.	9.4	142
28	Cobalt Nanoparticles Encapsulated in Porous Carbons Derived from Core–Shell ZIF67@ZIF8 as Efficient Electrocatalysts for Oxygen Evolution Reaction. ACS Applied Materials & Interfaces, 2017, 9, 28685-28694.	8.0	142
29	Structuring phase junction between tri-s-triazine and triazine crystalline C3N4 for efficient photocatalytic hydrogen evolution. Applied Catalysis B: Environmental, 2018, 227, 153-160.	20.2	139
30	Selective electrochemical H2O2 generation and activation on a bifunctional catalyst for heterogeneous electro-Fenton catalysis. Journal of Hazardous Materials, 2020, 382, 121102.	12.4	137
31	Enhanced heterogeneous activation of peroxymonosulfate by Co and N codoped porous carbon for degradation of organic pollutants: the synergism between Co and N. Environmental Science: Nano, 2019, 6, 399-410.	4.3	129
32	Enhanced Permeability, Selectivity, and Antifouling Ability of CNTs/Al ₂ O ₃ Membrane under Electrochemical Assistance. Environmental Science & Technology, 2015, 49, 2293-2300.	10.0	128
33	Fabrication of a TiO ₂ â^'BDD Heterojunction and its Application As a Photocatalyst for the Simultaneous Oxidation of an Azo Dye and Reduction of Cr(VI). Environmental Science & Samp; Technology, 2008, 42, 3791-3796.	10.0	121
34	Degradation of p-nitrophenol in aqueous solution by microwave assisted oxidation process through a granular activated carbon fixed bed. Water Research, 2006, 40, 3061-3068.	11.3	114
35	High-Efficiency Electrocatalysis of Molecular Oxygen toward Hydroxyl Radicals Enabled by an Atomically Dispersed Iron Catalyst. Environmental Science & Technology, 2020, 54, 12662-12672.	10.0	114
36	Facile Method for Fabricating Boron-Doped TiO ₂ Nanotube Array with Enhanced Photoelectrocatalytic Properties. Industrial & Engineering Chemistry Research, 2008, 47, 3804-3808.	3.7	107

#	Article	IF	CITATIONS
37	"Mulberry-like―CdSe Nanoclusters Anchored on TiO ₂ Nanotube Arrays: A Novel Architecture with Remarkable Photoelectrochemical Performance. Chemistry of Materials, 2009, 21, 3090-3095.	6.7	105
38	Integration of membrane filtration and photoelectrocatalysis on g-C3N4/CNTs/Al2O3 membrane with visible-light response for enhanced water treatment. Journal of Membrane Science, 2017, 541, 153-161.	8.2	105
39	Fabrication of Flexible Mesoporous Black Nb ₂ O ₅ Nanofiber Films for Visibleâ€Lightâ€Driven Photocatalytic CO ₂ Reduction into CH ₄ . Advanced Materials, 2022, 34, e2200756.	21.0	104
40	Tuning Lewis acidity of MIL-88B-Fe with mix-valence coordinatively unsaturated iron centers on ultrathin Ti3C2 nanosheets for efficient photo-Fenton reaction. Applied Catalysis B: Environmental, 2020, 264, 118534.	20.2	102
41	Constructing BiVO4-Au@CdS photocatalyst with energic charge-carrier-separation capacity derived from facet induction and Z-scheme bridge for degradation of organic pollutants. Applied Catalysis B: Environmental, 2018, 227, 258-265.	20.2	100
42	Carbon nitride with electron storage property: Enhanced exciton dissociation for high-efficient photocatalysis. Applied Catalysis B: Environmental, 2018, 236, 99-106.	20.2	99
43	Ferroelectric-enhanced Z-schematic electron transfer in BiVO 4 -BiFeO 3 -CuInS 2 for efficient photocatalytic pollutant degradation. Applied Catalysis B: Environmental, 2017, 209, 591-599.	20.2	96
44	An effective combination reaction involved with sputtered and selenized Sb precursors for efficient Sb2Se3 thin film solar cells. Chemical Engineering Journal, 2020, 393, 124599.	12.7	95
45	Electrochemically enhanced adsorption of aniline on activated carbon fibers. Separation and Purification Technology, 2006, 50, 365-372.	7.9	93
46	Enhanced electro-Fenton performance by fluorine-doped porous carbon for removal of organic pollutants in wastewater. Chemical Engineering Journal, 2018, 354, 606-615.	12.7	91
47	Enhanced Perfluorooctanoic Acid Degradation by Electrochemical Activation of Sulfate Solution on B/N Codoped Diamond. Environmental Science & Technology, 2019, 53, 5195-5201.	10.0	91
48	Nanocarbon-based membrane filtration integrated with electric field driving for effective membrane fouling mitigation. Water Research, 2016, 88, 285-292.	11.3	89
49	Efficient day-night photocatalysis performance of 2D/2D Ti3C2/Porous g-C3N4 nanolayers composite and its application in the degradation of organic pollutants. Chemosphere, 2020, 246, 125760.	8.2	89
50	Integration of separation and photocatalysis using an inorganic membrane modified with Si-doped TiO2 for water purification. Journal of Membrane Science, 2009, 335, 58-67.	8.2	84
51	Improving Ion Rejection of Conductive Nanofiltration Membrane through Electrically Enhanced Surface Charge Density. Environmental Science & Technology, 2019, 53, 868-877.	10.0	83
52	Rational band engineering and structural manipulations inducing high thermoelectric performance in n-type CoSb3 thin films. Nano Energy, 2021, 81, 105683.	16.0	82
53	Boron and Nitrogen Codoped Nanodiamond as an Efficient Metal-Free Catalyst for Oxygen Reduction Reaction. Journal of Physical Chemistry C, 2013, 117, 14992-14998.	3.1	80
54	Porous metal–organic framework MIL-100(Fe) as an efficient catalyst for the selective catalytic reduction of NO _x with NH ₃ . RSC Advances, 2014, 4, 48912-48919.	3.6	80

#	Article	IF	CITATIONS
55	Combined Effects of Surface Charge and Pore Size on Co-Enhanced Permeability and Ion Selectivity through RGO-OCNT Nanofiltration Membranes. Environmental Science & Technology, 2018, 52, 4827-4834.	10.0	79
56	Electrochemical Determination of Tetracycline Using Molecularly Imprinted Polymer Modified Carbon Nanotubeâ€Gold Nanoparticles Electrode. Electroanalysis, 2011, 23, 1863-1869.	2.9	77
57	Cobalt implanted TiO ₂ nanocatalyst for heterogeneous activation of peroxymonosulfate. RSC Advances, 2013, 3, 520-525.	3.6	77
58	Fluorine-doped carbon nanotubes as an efficient metal-free catalyst for destruction of organic pollutants in catalytic ozonation. Chemosphere, 2018, 190, 135-143.	8.2	75
59	Toxic effect of serial perfluorosulfonic and perfluorocarboxylic acids on the membrane system of a freshwater alga measured by flow cytometry. Environmental Toxicology and Chemistry, 2008, 27, 1597-1604.	4.3	72
60	Enhanced catalytic ozonation by highly dispersed CeO2 on carbon nanotubes for mineralization of organic pollutants. Journal of Hazardous Materials, 2019, 368, 621-629.	12.4	71
61	Enhanced Chlorinated Pollutant Degradation by the Synergistic Effect between Dechlorination and Hydroxyl Radical Oxidation on a Bimetallic Single-Atom Catalyst. Environmental Science & Technology, 2021, 55, 14194-14203.	10.0	70
62	Bioelectrochemical enhancement of anaerobic methanogenesis for high organic load rate wastewater treatment in a up-flow anaerobic sludge blanket (UASB) reactor. Scientific Reports, 2014, 4, 6658.	3.3	68
63	Enhanced catalytic activity over MIL-100(Fe) loaded ceria catalysts for the selective catalytic reduction of NO x with NH 3 at low temperature. Journal of Hazardous Materials, 2016, 301, 512-521.	12.4	68
64	Effective adsorption of sulfamethoxazole, bisphenol A and methyl orange on nanoporous carbon derived from metal-organic frameworks. Journal of Environmental Sciences, 2018, 63, 250-259.	6.1	68
65	Energy-transfer-mediated oxygen activation in carbonyl functionalized carbon nitride nanosheets for high-efficient photocatalytic water disinfection and organic pollutants degradation. Water Research, 2020, 177, 115798.	11.3	68
66	Degradation of aqueous bisphenol A in the CoCN/Vis/PMS system: Catalyst design, reaction kinetic and mechanism analysis. Chemical Engineering Journal, 2021, 407, 127228.	12.7	68
67	Recovery of Raman spectra with low signal-to-noise ratio using Wiener estimation. Optics Express, 2014, 22, 12102.	3.4	66
68	Facile Synthesis of γâ€In ₂ Se ₃ Nanoflowers toward High Performance Selfâ€Powered Broadband γâ€In ₂ Se ₃ /Si Heterojunction Photodiode. Small, 2017, 13, 1604033.	10.0	64
69	Thermally and electrically conductive multifunctional sensor based on epoxy/graphene composite. Nanotechnology, 2020, 31, 075702.	2.6	64
70	Electroluminescent materials toward near ultraviolet region. Chemical Society Reviews, 2021, 50, 8639-8668.	38.1	63
71	Dynamic adsorption of ciprofloxacin on carbon nanofibers: Quantitative measurement by in situ fluorescence. Journal of Water Process Engineering, 2016, 9, e14-e20.	5.6	61
72	Durable and Selective Electrochemical H ₂ O ₂ Synthesis under a Large Current Enabled by the Cathode with Highly Hydrophobic Three-Phase Architecture. ACS Catalysis, 2021, 11, 13797-13808.	11.2	59

#	Article	IF	CITATIONS
73	Highly Permeable Thin-Film Composite Forward Osmosis Membrane Based on Carbon Nanotube Hollow Fiber Scaffold with Electrically Enhanced Fouling Resistance. Environmental Science & Technology, 2018, 52, 1444-1452.	10.0	56
74	Preoperative Prediction of Axillary Lymph Node Metastasis in Breast Cancer using Radiomics Features of DCE-MRI. Scientific Reports, 2019, 9, 2240.	3.3	56
75	Reduction of acute toxicity and genotoxicity of dye effluent using Fenton-coagulation process. Journal of Hazardous Materials, 2014, 274, 198-204.	12.4	54
76	A State-of-the-Art Survey for Microorganism Image Segmentation Methods and Future Potential. IEEE Access, 2019, 7, 100243-100269.	4.2	53
77	Evaluation of the detoxification efficiencies of coking wastewater treated by combined anaerobic-anoxic-oxic (A 2 O) and advanced oxidation process. Journal of Hazardous Materials, 2017, 338, 186-193.	12.4	52
78	Electrochemical reduction of N ₂ to ammonia on Co single atom embedded N-doped porous carbon under ambient conditions. Journal of Materials Chemistry A, 2019, 7, 26358-26363.	10.3	51
79	Integration of membrane filtration and photoelectrocatalysis using a TiO2/carbon/Al2O3 membrane for enhanced water treatment. Journal of Hazardous Materials, 2015, 299, 27-34.	12.4	50
80	An electrochemical sensor for selective determination of sulfamethoxazole in surface water using a molecularly imprinted polymer modified BDD electrode. Analytical Methods, 2015, 7, 2693-2698.	2.7	50
81	Impact of dissolved organic matter on the photolysis of the ionizable antibiotic norfloxacin. Journal of Environmental Sciences, 2015, 27, 115-123.	6.1	50
82	Enhanced separation performance of carbon nanotube–polyvinyl alcohol composite membranes for emulsified oily wastewater treatment under electrical assistance. Separation and Purification Technology, 2018, 197, 107-115.	7.9	50
83	Efficient and stable heterogeneous electro-Fenton system using iron oxides embedded in Cu, N co-doped hollow porous carbon as functional electrocatalyst. Separation and Purification Technology, 2020, 238, 116424.	7.9	50
84	Carbon nanotubes-incorporated MIL-88B-Fe as highly efficient Fenton-like catalyst for degradation of organic pollutants. Frontiers of Environmental Science and Engineering, 2019, 13, 1.	6.0	49
85	Highly efficient metal-free electro-Fenton degradation of organic contaminants on a bifunctional catalyst. Journal of Hazardous Materials, 2021, 416, 125859.	12.4	49
86	Facile synthesis of hybrid nanorods with the Sb ₂ Se ₃ /AgSbSe ₂ heterojunction structure for high performance photodetectors. Nanoscale, 2016, 8, 2277-2283.	5.6	48
87	α-Cu2Se thermoelectric thin films prepared by copper sputtering into selenium precursor layers. Chemical Engineering Journal, 2021, 410, 128444.	12.7	48
88	Enhanced degradation of organic water pollutants by photocatalytic in-situ activation of sulfate based on Z-scheme g-C3N4/BiPO4. Chemical Engineering Journal, 2022, 428, 132116.	12.7	48
89	Enhanced adsorption of ionizable antibiotics on activated carbon fiber under electrochemical assistance in continuous-flow modes. Water Research, 2018, 134, 162-169.	11.3	47
90	Two-Dimensional Lead Monoxide: Facile Liquid Phase Exfoliation, Excellent Photoresponse Performance, and Theoretical Investigation. ACS Photonics, 2018, 5, 5055-5067.	6.6	47

#	Article	IF	CITATIONS
91	Fabrication of graphene wrapped ZnIn2S4microspheres heterojunction with enhanced interfacial contact and its improved photocatalytic performance. Dalton Transactions, 2014, 43, 2888-2894.	3.3	46
92	Superpermeable Atomic-Thin Graphene Membranes with High Selectivity. ACS Nano, 2017, 11, 1920-1926.	14.6	45
93	Improvement of Antifouling and Antimicrobial Abilities on Silver–Carbon Nanotube Based Membranes under Electrochemical Assistance. Environmental Science & Technology, 2019, 53, 5292-5300.	10.0	45
94	Modified Wiener estimation of diffuse reflectance spectra from RGB values by the synthesis of new colors for tissue measurements. Journal of Biomedical Optics, 2012, 17, 030501.	2.6	44
95	Electrochemiluminescence immunosensor for highly sensitive detection of 8-hydroxy-2′-deoxyguanosine based on carbon quantum dot coated Au/SiO2 core–shell nanoparticles. Talanta, 2015, 131, 379-385.	5.5	44
96	Synthesis of manganese incorporated hierarchical mesoporous silica nanosphere with fibrous morphology by facile one-pot approach for efficient catalytic ozonation. Journal of Hazardous Materials, 2016, 318, 308-318.	12.4	44
97	Operating redox couple transport mechanism for enhancing photocatalytic H2 generation of Pt and CrOx-decorated ZnCdS nanocrystals. Applied Catalysis B: Environmental, 2021, 283, 119601.	20.2	44
98	Identifying non-muscle-invasive and muscle-invasive bladder cancer based on blood serum surface-enhanced Raman spectroscopy. Biomedical Optics Express, 2019, 10, 3533.	2.9	43
99	Nitrogen-doped diamond electrode shows high performance for electrochemical reduction of nitrobenzene. Journal of Hazardous Materials, 2014, 265, 185-190.	12.4	41
100	Enhancement of anaerobic acidogenesis by integrating an electrochemical system into an acidogenic reactor: Effect of hydraulic retention times (HRT) and role of bacteria and acidophilic methanogenic Archaea. Bioresource Technology, 2015, 179, 43-49.	9.6	40
101	Low-cost fabrication of a paper-based microfluidic using a folded pattern paper. Analytica Chimica Acta, 2019, 1053, 131-138.	5.4	40
102	Fabrication of Sb2S3 thin films by magnetron sputtering and post-sulfurization/selenization for substrate structured solar cells. Journal of Alloys and Compounds, 2020, 826, 154235.	5.5	40
103	Three-Dimensional Porous H _{<i>x</i>} TiS ₂ Nanosheet–Polyaniline Nanocomposite Electrodes for Directly Detecting Trace Cu(II) Ions. Analytical Chemistry, 2015, 87, 5605-5613.	6.5	39
104	Analysis and classification of kidney stones based on Raman spectroscopy. Biomedical Optics Express, 2018, 9, 4175.	2.9	39
105	Carbon nanotube hollow fiber membranes: High-throughput fabrication, structural control and electrochemically improved selectivity. Journal of Membrane Science, 2015, 493, 97-105.	8.2	38
106	Photoelectrochemical aptasensor for sulfadimethoxine using g-C3N4 quantum dots modified with reduced graphene oxide. Mikrochimica Acta, 2018, 185, 345.	5.0	38
107	Temperature-difference-induced electricity during solar desalination with bilayer MXene-based monoliths. Nano Energy, 2020, 76, 105060.	16.0	37
108	In situ controllable growth of noble metal nanodot on graphene sheet. Journal of Materials Chemistry, 2011, 21, 12986.	6.7	36

#	Article	IF	CITATIONS
109	Enhancing anaerobic digestion in anaerobic integrated floating fixed-film activated sludge (An-IFFAS) system using novel electron mediator suspended biofilm carriers. Water Research, 2020, 175, 115697.	11.3	36
110	Efficient electrochemical nitrate removal on Cu and nitrogen doped carbon. Chemical Engineering Journal, 2021, 415, 128958.	12.7	36
111	Photochemical Formation of Hydroxylated Polybrominated Diphenyl Ethers (OH-PBDEs) from Polybrominated Diphenyl Ethers (PBDEs) in Aqueous Solution under Simulated Solar Light Irradiation. Environmental Science & Technology, 2015, 49, 9092-9099.	10.0	35
112	Assessing the effectiveness of artificial intelligence methods for melanoma: A retrospective review. Journal of the American Academy of Dermatology, 2019, 81, 1176-1180.	1.2	35
113	Stepwise method based on Wiener estimation for spectral reconstruction in spectroscopic Raman imaging. Optics Express, 2017, 25, 1005.	3.4	34
114	Enhanced electrical conductivity and photoconductive properties of Sn-doped Sb ₂ Se ₃ crystals. Journal of Materials Chemistry C, 2018, 6, 6465-6470.	5.5	34
115	Fabrication of Au/CNT hollow fiber membrane for 4-nitrophenol reduction. RSC Advances, 2016, 6, 41114-41121.	3.6	33
116	Electrokinetic Enhancement of Water Flux and Ion Rejection through Graphene Oxide/Carbon Nanotube Membrane. Environmental Science & Technology, 2020, 54, 15433-15441.	10.0	33
117	Magnetron sputtered Sb2Se3-based thin films towards high performance quasi-homojunction thin film solar cells. Solar Energy Materials and Solar Cells, 2019, 203, 110154.	6.2	32
118	Electrochemical activation of peroxymonosulfate in cathodic micro-channels for effective degradation of organic pollutants in wastewater. Journal of Hazardous Materials, 2020, 398, 122879.	12.4	31
119	Low-Cost and Highly Sensitive Wearable Sensor Based on Napkin for Health Monitoring. Sensors, 2019, 19, 3427.	3.8	30
120	Porous carbon membrane with enhanced selectivity and antifouling capability for water treatment under electrochemical assistance. Journal of Colloid and Interface Science, 2020, 560, 59-68.	9.4	30
121	Construction of a Microchannel Electrochemical Reactor with a Monolithic Porous-Carbon Cathode for Adsorption and Degradation of Organic Pollutants in Several Minutes of Retention Time. Environmental Science & amp; Technology, 2020, 54, 1920-1928.	10.0	30
122	Fundamental Physical Characterization of Sb ₂ Se ₃ -Based Quasi-Homojunction Thin Film Solar Cells. ACS Applied Materials & Interfaces, 2020, 12, 30572-30583.	8.0	30
123	Flow-through heterogeneous electro-Fenton system based on the absorbent cotton derived bulk electrode for refractory organic pollutants treatment. Separation and Purification Technology, 2021, 276, 119266.	7.9	30
124	Serum microRNA-221 as a biomarker for diabetic retinopathy in patients associated with type 2 diabetes. International Journal of Ophthalmology, 2018, 11, 1889-1894.	1.1	29
125	High-performance bismuth telluride thermoelectric thin films fabricated by using the two-step single-source thermal evaporation. Journal of Alloys and Compounds, 2020, 819, 153027.	5.5	29
126	High Openâ€Circuit Voltage in Fullâ€Inorganic Sb ₂ S ₃ Solar Cell via Modified Znâ€Doped TiO ₂ Electron Transport Layer. Solar Rrl, 2020, 4, 2000551.	5.8	29

#	Article	IF	CITATIONS
127	Constructing metal-free polyimide/g-C ₃ N ₄ with high photocatalytic activity under visible light irradiation. RSC Advances, 2015, 5, 83225-83231.	3.6	28
128	Enhanced activation of peroxymonosulfate by CNT-TiO2 under UV-light assistance for efficient degradation of organic pollutants. Frontiers of Environmental Science and Engineering, 2019, 13, 1.	6.0	28
129	Electro-assisted CNTs/ceramic flat sheet ultrafiltration membrane for enhanced antifouling and separation performance. Frontiers of Environmental Science and Engineering, 2021, 15, 1.	6.0	27
130	A ZIF-8-based platform for the rapid and highly sensitive detection of indoor formaldehyde. RSC Advances, 2014, 4, 36444-36450.	3.6	26
131	Nutrient removal performance and microbial characteristics of a full-scale IFAS-EBPR process treating municipal wastewater. Water Science and Technology, 2016, 73, 1261-1268.	2.5	26
132	Enhanced heterogeneous Fenton-like activity by Cu-doped BiFeO3 perovskite for degradation of organic pollutants. Frontiers of Environmental Science and Engineering, 2018, 12, 1.	6.0	26
133	Fast reconstruction of Raman spectra from narrowâ€band measurements based on Wiener estimation. Journal of Raman Spectroscopy, 2013, 44, 875-881.	2.5	25
134	Efficient electrochemical reduction of nitrobenzene by nitrogen doped porous carbon. Chemosphere, 2020, 238, 124636.	8.2	25
135	Detecting urine metabolites of bladder cancer by surface-enhanced Raman spectroscopy. Spectrochimica Acta - Part A: Molecular and Biomolecular Spectroscopy, 2021, 247, 119108.	3.9	25
136	Exquisite Enzyme-Fenton Biomimetic Catalysts for Hydroxyl Radical Production by Mimicking an Enzyme Cascade. ACS Applied Materials & Interfaces, 2018, 10, 8666-8675.	8.0	24
137	A high performance broadband photodetector based on (Sn _x Sb _{1â^'x}) ₂ Se ₃ nanorods with enhanced electrical conductivity. Journal of Materials Chemistry C, 2018, 6, 11078-11085.	5.5	24
138	Photocatalytic ozonation of organic pollutants in wastewater using a flowing through reactor. Journal of Hazardous Materials, 2021, 405, 124277.	12.4	24
139	Photochemical transformation of 2,2′,4,4′-tetrabromodiphenyl ether (BDE-47) in surface coastal waters: Effects of chloride and ferric ions. Marine Pollution Bulletin, 2014, 86, 76-83.	5.0	23
140	Comparison of CNT-PVA membrane and commercial polymeric membranes in treatment of emulsified oily wastewater. Frontiers of Environmental Science and Engineering, 2019, 13, 1.	6.0	23
141	Constructing efficient WO3-FPC system for photoelectrochemical H2O2 production and organic pollutants degradation. Chemical Engineering Journal, 2020, 389, 123427.	12.7	23
142	Fabrication of FeOCl nanoparticles modified microchannel carbon cathode for flow-through electro-Fenton degradation of refractory organic pollutants. Separation and Purification Technology, 2022, 288, 120661.	7.9	23
143	Identifying benign and malignant thyroid nodules based on blood serum surface-enhanced Raman spectroscopy. Nanomedicine: Nanotechnology, Biology, and Medicine, 2021, 32, 102328.	3.3	22
144	Treatment of organic wastewater by a synergic electrocatalysis process with Ti3+ self-doped TiO2 nanotube arrays electrode as both cathode and anode. Journal of Hazardous Materials, 2022, 424, 127747.	12.4	22

#	Article	IF	CITATIONS
145	Poly(vinylidene fluoride) hollowâ€fiber membranes containing silver/graphene oxide dope with excellent filtration performance. Journal of Applied Polymer Science, 2017, 134, .	2.6	21
146	Label-free detection of multiple genitourinary cancers from urine by surface-enhanced Raman spectroscopy. Spectrochimica Acta - Part A: Molecular and Biomolecular Spectroscopy, 2020, 240, 118543.	3.9	20
147	Fabrication of graphitic-C ₃ N ₄ quantum dots coated silicon nanowire array as a photoelectrode for vigorous degradation of 4-chlorophenol. RSC Advances, 2017, 7, 14832-14836.	3.6	19
148	Examining the Interfacial Defect Passivation with Chlorinated Organic Salt for Highly Efficient and Stable Perovskite Solar Cells. Solar Rrl, 2020, 4, 2000358.	5.8	19
149	Nanoplating of a SnO ₂ thin-film on MXene-based sponge for stable and efficient solar energy conversion. Journal of Materials Chemistry A, 2020, 8, 8065-8074.	10.3	19
150	Competitive adsorption and desorption of copper and lead in some soil of North China. Frontiers of Environmental Science and Engineering, 2012, 6, 484-492.	6.0	18
151	Optimization of advanced Wiener estimation methods for Raman reconstruction from narrow-band measurements in the presence of fluorescence background. Biomedical Optics Express, 2015, 6, 2633.	2.9	18
152	Anaerobic biodecolorization of AO7 by a newly isolated Fe(III)-reducing bacterium <i>Sphingomonas</i> strain DJ. Journal of Chemical Technology and Biotechnology, 2015, 90, 158-165.	3.2	18
153	Fast wide-field Raman spectroscopic imaging based on simultaneous multi-channel image acquisition and Wiener estimation. Optics Letters, 2016, 41, 2783.	3.3	18
154	Electrochemically enhanced adsorption of PFOA and PFOS on multiwalled carbon nanotubes in continuous flow mode. Science Bulletin, 2014, 59, 2890-2897.	1.7	17
155	Spark plasma sintering of Sb2Se3 sputtering target towards highly efficient thin film solar cells. Solar Energy Materials and Solar Cells, 2020, 211, 110530.	6.2	17
156	Enhanced Photodegradation of PNP on Soil Surface under UV Irradiation with TiO2. Soil and Sediment Contamination, 2007, 16, 413-421.	1.9	16
157	Tuning the electrochemical properties of a boron and nitrogen codoped nanodiamond rod array to achieve high performance for both electro-oxidation and electro-reduction. Journal of Materials Chemistry A, 2013, 1, 14706.	10.3	16
158	Enhanced anaerobic fermentation with azo dye as electron acceptor: Simultaneous acceleration of organics decomposition and azo decolorization. Journal of Environmental Sciences, 2014, 26, 1970-1976.	6.1	16
159	A surface plasmon-enhanced nanozyme-based fenton process for visible-light-driven aqueous ammonia oxidation. Green Chemistry, 2018, 20, 4067-4074.	9.0	16
160	Selective reduction of nitrate to ammonium over charcoal electrode derived from natural wood. Chemosphere, 2021, 285, 131501.	8.2	16
161	Preparation and characterization of aligned carbon nanotubes coated with titania nanoparticles. Science Bulletin, 2006, 51, 2294-2296.	1.7	14
162	Early Prediction of Skin Viability Using Visible Diffuse Reflectance Spectroscopy and Autofluorescence Spectroscopy. Plastic and Reconstructive Surgery, 2014, 134, 240e-247e.	1.4	14

#	Article	IF	CITATIONS
163	Voltage-Gated Transport of Nanoparticles across Free-Standing All-Carbon-Nanotube-Based Hollow-Fiber Membranes. ACS Applied Materials & Interfaces, 2015, 7, 14620-14627.	8.0	14
164	Enhancing nitrogen removal efficiency and reducing nitrate liquor recirculation ratio by improving simultaneous nitrification and denitrification in integrated fixed-film activated sludge (IFAS) process. Water Science and Technology, 2016, 73, 827-834.	2.5	14
165	Acute toxicity reduction and toxicity identification in pigment-contaminated wastewater during anaerobic-anoxic-oxic (A/A/O) treatment process. Chemosphere, 2017, 168, 1285-1292.	8.2	14
166	Micron-Scale Photodetectors Based on One-Dimensional Single-Crystalline Sb2–xSnxSe3 Microrods: Simultaneously Improving Responsivity and Extending Spectral Response Region. Journal of Physical Chemistry C, 2019, 123, 810-816.	3.1	14
167	Construction of a Microchannel Aeration Cathode for Producing H ₂ O ₂ via Oxygen Reduction Reaction. ACS Applied Materials & Interfaces, 2021, 13, 56045-56053.	8.0	14
168	A Fast Fluorescence Background Suppression Method for Raman Spectroscopy Based on Stepwise Spectral Reconstruction. IEEE Access, 2018, 6, 67709-67717.	4.2	13
169	Enhanced nitrification in integrated floating fixed-film activated sludge (IFFAS) system using novel clinoptilolite composite carrier. Frontiers of Environmental Science and Engineering, 2019, 13, 1.	6.0	13
170	Structure, Morphology, and Photoelectric Performances of Te-Sb2Se3 Thin Film Prepared via Magnetron Sputtering. Nanomaterials, 2020, 10, 1358.	4.1	13
171	Evaluation of the detoxication efficiencies for acrylonitrile wastewater treated by a combined anaerobic oxic-aerobic biological fluidized tank (A/O-ABFT) process: Acute toxicity and zebrafish embryo toxicity. Chemosphere, 2016, 154, 1-7.	8.2	12
172	Performing homogeneous catalytic ozonation using heterogeneous Mn ²⁺ -bonded oxidized carbon nanotubes by self-driven pH variation induced reversible desorption and adsorption of Mn ²⁺ . Environmental Science: Nano, 2019, 6, 1932-1940.	4.3	12
173	Electroconductive RGO-MXene membranes with wettability-regulated channels: improved water permeability and electro-enhanced rejection performance. Frontiers of Environmental Science and Engineering, 2023, 17, .	6.0	12
174	Fabrication of needle-like ZnO nanorods arrays by a low-temperature seed-layer growth approach in solution. Applied Physics A: Materials Science and Processing, 2007, 89, 673-679.	2.3	11
175	Early detection and differentiation of venous and arterial occlusion in skin flaps using visible diffuse reflectance spectroscopy and autofluorescence spectroscopy. Biomedical Optics Express, 2016, 7, 570.	2.9	11
176	Weighted spectral reconstruction method for discrimination of bacterial species with low signal-to-noise ratio Raman measurements. RSC Advances, 2019, 9, 9500-9508.	3.6	11
177	Efficient Light-Driven Fuel Cell with Simultaneous Degradation of Pollutants on a TiO ₂ Photoanode and Production of H ₂ O ₂ on a Gas Diffusion Electrode Cathode. ACS ES&T Engineering, 2021, 1, 1122-1130.	7.6	11
178	Reducing livestock snow disaster risk in the Qinghai–Tibetan Plateau due to warming and socioeconomic development. Science of the Total Environment, 2022, 813, 151869.	8.0	11
179	Dataset of trend-preserving bias-corrected daily temperature, precipitation and wind from NEX-GDDP and CMIP5 over the Qinghai-Tibet Plateau. Data in Brief, 2020, 31, 105733.	1.0	10
180	Ultrasensitive immunoassay of microcystins-LR using G-quadruplex DNAzyme as an electrocatalyst. International Journal of Environmental Analytical Chemistry, 2014, 94, 988-1000.	3.3	9

#	Article	IF	CITATIONS
181	Spectral diffuse reflectance and autofluorescence imaging can perform early prediction of blood vessel occlusion in skin flaps. Journal of Biophotonics, 2017, 10, 1665-1675.	2.3	9
182	Synthesis and properties of strong and tough Diels–Alder self-healing crosslinked polyamides. Journal of Polymer Research, 2021, 28, 1.	2.4	9
183	Identifying functioning and nonfunctioning adrenal tumors based on blood serum surface-enhanced Raman spectroscopy. Analytical and Bioanalytical Chemistry, 2021, 413, 4289-4299.	3.7	9
184	Identification and assessment of pulmonary Cryptococcus neoformans infection by blood serum surface-enhanced Raman spectroscopy. Spectrochimica Acta - Part A: Molecular and Biomolecular Spectroscopy, 2021, 260, 119978.	3.9	9
185	Effects of humic acid fractions with different polarities on photodegradation of 2,4-D in aqueous environments. Frontiers of Environmental Science and Engineering in China, 2008, 2, 291-296.	0.8	8
186	Electrocatalytic dechlorination of 2,4,5-trichlorobiphenyl using an aligned carbon nanotubes electrode deposited with palladium nanoparticles. Science Bulletin, 2010, 55, 358-364.	1.7	8
187	Software controlling algorithms for the system performance optimization of confocal laser scanning microscope. Biomedical Signal Processing and Control, 2010, 5, 223-228.	5.7	8
188	Green Synthesis of Feather-Shaped MoS ₂ /CdS Photocatalyst for Effective Hydrogen Production. International Journal of Photoenergy, 2013, 2013, 1-5.	2.5	8
189	Production of dimethylsulfide and acrylic acid from dimethylsulfoniopropionate during growth of three marine microalgae. Chinese Journal of Oceanology and Limnology, 2014, 32, 1270-1279.	0.7	8
190	Superpermeable nanoporous carbon-based catalytic membranes for electro-Fenton driven high-efficiency water treatment. Journal of Materials Chemistry A, 2018, 6, 23502-23512.	10.3	8
191	Efficient H2O2 generation and electro-Fenton degradation of pollutants in microchannels of oxidized monolithic-porous-carbon cathode. Water Science and Technology, 2019, 80, 970-978.	2.5	8
192	Covering α-Fe2O3 protection layer on the surface of p-Si micropillar array for enhanced photoelectrochemical performance. Frontiers of Environmental Science and Engineering, 2017, 11, 1.	6.0	7
193	Enhancing nitrogen removal efficiency in a dyestuff wastewater treatment plant with the IFFAS process: the pilot-scale and full-scale studies. Water Science and Technology, 2018, 77, 70-78.	2.5	7
194	Preparation of antimonene nanosheets and their thermoelectric nanocomposites. Composites Communications, 2021, 28, 100968.	6.3	7
195	Salt-controlled assembly of stacked-graphene for capturing fluorescence and its application in chemical genotoxicity screening. Journal of Materials Chemistry, 2011, 21, 15266.	6.7	6
196	Enhancing nitrogen and phosphorus removal in the BUCT–IFAS process by bypass flow strategy. Water Science and Technology, 2015, 72, 528-534.	2.5	6
197	Fast temperature estimation from undersampled k-space with fully-sampled center for MR guided microwave ablation. Magnetic Resonance Imaging, 2016, 34, 1171-1180.	1.8	6
198	A Method to Create a Universal Calibration Dataset for Raman Reconstruction Based on Wiener Estimation. IEEE Journal of Selected Topics in Quantum Electronics, 2016, 22, 164-170.	2.9	6

#	Article	IF	CITATIONS
199	Rapid and sensitive detection of Acidovorax citrulli in cucurbit seeds by visual loopâ€mediated isothermal amplification assay. Journal of Phytopathology, 2019, 167, 10-18.	1.0	6
200	Synthesis and properties of selfâ€healing crossâ€linked nonisocyanate polyurethanes from biobased diglycerol bis(cyclic carbonate). Polymer Engineering and Science, 2021, 61, 497-505.	3.1	6
201	Catalyzed Michael addition, polycondensation, and the related performance of Diels–Alder selfâ€healing crosslinked polyamides. Polymer Engineering and Science, 2022, 62, 1269-1280.	3.1	6
202	High-efficiency electrochemical activation of H2O2 into ·OH enabled by flow-through FeOCl-modified carbon electrode for organic pollutants degradation. Separation and Purification Technology, 2022, 295, 121279.	7.9	6
203	Photodegradation of 2,4-D induced by NO2â^' in aqueous solutions: The role of NO2. Journal of Environmental Sciences, 2014, 26, 1383-1387.	6.1	5
204	Direct growth of ultra-permeable molecularly thin porous graphene membranes for water treatment. Environmental Science: Nano, 2018, 5, 3004-3010.	4.3	5
205	Effect of organic nano-components on the thermoelectric properties of Sb2Te3 nanocrystal thin film. Scripta Materialia, 2020, 185, 105-110.	5.2	5
206	Predicting Unnecessary Nodule Biopsies from a Small, Unbalanced, and Pathologically Proven Dataset by Transfer Learning. Journal of Digital Imaging, 2020, 33, 685-696.	2.9	5
207	Tortuosity of Retinal Main and Branching Arterioles, Venules in Patients With Type 2 Diabetes and Diabetic Retinopathy in China. IEEE Access, 2020, 8, 6201-6208.	4.2	5
208	Predicting prognosis in acute myeloid leukemia patients by surface-enhanced Raman spectroscopy. Nanomedicine, 2021, 16, 1873-1885.	3.3	5
209	Early assessment of chemotherapeutic response in hepatocellular carcinoma based on serum surface-enhanced Raman spectroscopy. Spectrochimica Acta - Part A: Molecular and Biomolecular Spectroscopy, 2022, 278, 121314.	3.9	5
210	Sequential weighted Wiener estimation for extraction of key tissue parameters in color imaging: a phantom study. Journal of Biomedical Optics, 2014, 19, 127001.	2.6	4
211	Accelerated model-based proton resonance frequency shift temperature mapping using echo-based GRAPPA reconstruction. Magnetic Resonance Imaging, 2015, 33, 240-245.	1.8	4
212	A Programmable Optical Filter With Arbitrary Transmittance for Fast Spectroscopic Imaging and Spectral Data Post-Processing. IEEE Access, 2019, 7, 119294-119308.	4.2	4
213	Utilizing transparent and conductive SnO2 as electron mediator to enhance the photocatalytic performance of Z-scheme Si-SnO2-TiOx. Frontiers of Environmental Science and Engineering, 2020, 14, 1.	6.0	4
214	Accelerating Monte Carlo simulation of light propagation in tissue mimicking turbid medium based on generative adversarial networks. Medical Physics, 2021, , .	3.0	4
215	Prediction of the postoperative prognosis in patients with non-muscle-invasive bladder cancer based on preoperative serum surface-enhanced Raman spectroscopy. Biomedical Optics Express, 2022, 13, 4204.	2.9	4
216	Fabrication of TiOx–Si photoanode and its energetic photoelectrochemical performance. Journal of Materials Science: Materials in Electronics, 2018, 29, 12700-12706.	2.2	3

#	Article	IF	CITATIONS
217	Mechanical properties and reaction products of reactive magnesia and CFB slag/silica fume pastes. Advances in Cement Research, 2019, 31, 297-307.	1.6	3
218	Templated nanoreactor arrays for nanoscale-tunable liquid-phase catalysis. Chemical Communications, 2019, 55, 6575-6578.	4.1	3
219	Enhanced thermoelectric properties of Sb2Te3/CH3NH3I hybrid thin films by post-annealing. Inorganic Chemistry Frontiers, 2020, 7, 198-203.	6.0	3
220	A surface-enhanced Raman scattering-based probe method for detecting chromogranin A in adrenal tumors. Nanomedicine, 2020, 15, 397-407.	3.3	3
221	Coding Convolutional Neural Networks as Spectral Transmittance for Intelligent Hyperspectral Remote Sensing in a Snapshot. IEEE Geoscience and Remote Sensing Letters, 2021, 18, 1635-1639.	3.1	3
222	Flexible Self-healing Cross-linked Polyamides Synthesized Through Bulk Michael Addition, Polycondensation, and Diels-Alder Reaction. Chemical Research in Chinese Universities, 0, , 1.	2.6	3
223	Importance of Environmental Black Carbon to Dissolved Petroleum Hydrocarbons Sorption on Soil. Soil and Sediment Contamination, 2009, 18, 184-194.	1.9	2
224	Electrocatalytic debromination of BDE-47 at palladized graphene electrode. Frontiers of Environmental Science and Engineering, 2014, 8, 180-187.	6.0	2
225	Epipolar geometry for prism-based single-lens stereovision. Machine Vision and Applications, 2017, 28, 313-326.	2.7	2
226	Programmable hyperspectral microscopy for high-contrast biomedical imaging in a snapshot. Journal of Biomedical Optics, 2020, 25, 1.	2.6	2
227	Influence of Temperature and Oil Content on the Soil/Air Partition Coefficient for Hexachlorobenzene in Oil-Contaminated Rice Paddy Field Soil. Soil and Sediment Contamination, 2011, 20, 221-233.	1.9	1
228	Experimental Study on Atomizing and Reaction Performance of Pressure Swirl Nozzles in Ethoxylation Reactor. International Journal of Chemical Reactor Engineering, 2016, 14, 965-974.	1.1	1
229	Innentitelbild: Selective Electrochemical Reduction of Carbon Dioxide to Ethanol on a Boron―and Nitrogenâ€Coâ€doped Nanodiamond (Angew. Chem. 49/2017). Angewandte Chemie, 2017, 129, 15678-15678.	2.0	1
230	Design of a Single-Lens Freeform-Prism-Based Distortion-Free Stereovision System. IEEE Photonics Journal, 2019, 11, 1-10.	2.0	1
231	Fabrication of a doubleâ€helical photocatalytic module for disinfection and antibiotics degradation. Water Environment Research, 2019, 91, 918-925.	2.7	1
232	Implementation and Test of an IEC 61850-Based Automation Framework for the Automated Data Model Integration of DES (ADMID) into DSO SCADA. Energies, 2022, 15, 1552.	3.1	1
233	High Spectral Resolution Raman Measurements Using Light-Emitting Diode as Excitation Based on Weighted Spectral Reconstruction Method. IEEE Access, 2019, 7, 134828-134837.	4.2	0
234	Reinforcement Learning for QoS-Constrained Autonomous Resource Allocation with H2H/M2M Co-Existence in Cellular Networks. IEICE Transactions on Communications, 2022, E105.B, 1332-1341.	0.7	0

#	Article	IF	CITATIONS
235	MTST: A splitting strategy to reduce the number of filters in programmable hyperspectral imaging for fast multi-target classification. Optics Express, 0, , .	3.4	0